

Tearing mode stability with equilibrium flows in the reversed-field pinch

R. Gatto¹, P.W. Terry¹ and C.C. Hegna²

¹ Department of Physics, University of Wisconsin-Madison, Madison, WI 53706, USA

² Department of Engineering Physics and Physics, University of Wisconsin-Madison, Madison, WI 53706, USA

E-mail: rgatto@facstaff.wisc.edu

Received 9 October 2001, accepted for publication 23 January 2002

Published 17 May 2002

Online at stacks.iop.org/NF/42/496

Abstract

The influence of certain equilibrium flows on the stability of tearing modes in the reversed-field pinch is investigated. By solving the linearized magnetohydrodynamic equations in cylindrical geometry, the tearing mode stability factor Δ' is calculated for a variety of axial flow profiles which have nonzero shear away from the rational surface, including flows localized entirely in the external, ideal region of the tearing mode. It is found that both $m = 1$ and $m = 0$ modes are destabilized by an axial flow localized near the edge of the plasma. This is the kind of flow that might be generated by any physical process creating an edge-localized radial electric field. A global flow profile with shear over the middle region of the plasma, simulating the differential rotation of core and edge modes observed in some reversed-field pinch discharges, is found to have a destabilizing effect on the $m = 1$ mode, while leaving the stability parameter of the $m = 0$ mode practically unchanged. The possible connection of these results with features of the spontaneous enhanced confinement regime in the Madison Symmetric Torus is discussed.

PACS numbers: 52.55.Lf, 52.55.-s

1. Introduction

Tearing mode activity plays an important role in the evolution of magnetic confinement discharges. This is particularly true for the reversed-field pinch (RFP), a toroidal device which, in contrast to the tokamak, has toroidal and poloidal magnetic fields of comparable magnitude. This makes the radial profile of the q -factor less than unity everywhere, and global tearing modes are unstable. In the RFP, large-scale magnetic fluctuations associated with tearing modes govern both particle [1] and energy [2] transport in the plasma core. Tearing modes also drive a nonlinear dynamo responsible for the reversal of the toroidal field [3], and produce bursty plasma relaxations (RFP sawteeth) [4–7]. Torques generated by the nonlinear interaction of tearing instabilities on different rational surfaces regulate the global momentum balance, and periodically brake plasma rotation during sawtooth events [8, 9]. Finally, Reynolds stress associated with tearing modes may generate regions of flow shear localized around mode rational surfaces [10].

In order to understand the complex dynamics of magnetic confinement discharges it is important to consider how these tearing mode-induced phenomena in turn affect the stability of the tearing mode. For example, the enhancement of the transport due to the magnetic turbulence generated when

magnetic islands overlap leads to modifications of the plasma profiles, which in turn affects the stability of tearing modes. This interaction between transport and resistive instability has been, and continues to be, a subject of study both in tokamak and RFP research. In the tokamak case this interaction is relevant to the onset of disruptions [11, 12]. In the RFP, it underlies the tendency of the plasma to relax to a state with reduced free energy and fluctuations [13, 14]. Another important, though less studied, example is the link between regions of shear flow, which are created by linear and nonlinear effects associated with tearing modes, or by other physical processes, and the modification of the stability of tearing modes due to such flows.

An RFP regime in which the dynamical interplay between tearing modes and flows may play an important role is the spontaneous enhanced confinement (EC) regime [15, 16] observed in the Madison Symmetric Torus (MST) [17]. This regime bears some similarities to the tokamak high-confinement, or H-mode, regime, which also can be generated spontaneously [18]. Although the mechanisms that lead to, and maintain a spontaneous EC discharge are not completely understood, a number of reproducible features are evident from experimental data. The spontaneous EC regime sets up following a sawtooth crash in discharges with sufficiently strong toroidal magnetic field reversal. The crash in the

RFP consists of a sudden increase of the $m = 1$ modes, which is followed almost immediately by a corresponding increase in the $m = 0$ mode. The increased activity of these modes induces an effective nonlinear torque which momentarily modifies the rotation of the plasma. Away from crashes, the plasma rotation is characterized by a flow profile that increases in going from the edge of the plasma inward. The torque due to the crash-induced nonlinear interaction of core $m = 1$ and edge $m = 0$ modes slows down the core modes, thus leading to a rigid-rotor-like plasma rotation. As the increased level of magnetic fluctuations decays to its pre-crash value, and the plasma rotation returns to its pre-crash pattern, some discharges bifurcate into an EC regime. Among the characteristics of this regime are a reduced level of magnetic and electrostatic fluctuations, the presence of an $E \times B$ shear flow localized at the edge of the plasma, and the occurrence of periodic bursts of $m = 0$ activity. Moreover, some spontaneous EC regimes enter a quasi-single-helicity (QSH) state, i.e. a state in which the magnetic fluctuation spectrum is dominated by the innermost resonant $m = 1$ mode. Spontaneous EC regimes have been observed to last up to 20 ms.

In this work we investigate the interaction between regions of sheared plasma flow and tearing mode stability in the MST spontaneous EC discharge. The principal objective is to determine whether or not the effect of shear flow on the stability of tearing modes could offer an explanation to some of the peculiar features of these discharges. To address this possibility, we consider the linearized ideal magnetohydrodynamic (MHD) model in cylindrical geometry, and calculate the tearing mode stability factor Δ' in the presence of equilibrium flows. We use flow profiles which mimic both the localized shear flow and the more global-scale rotation profile observed in the spontaneous EC regime. The numerical calculations of the stability factor carried out in this work are based entirely on linear theory. Even though tearing modes enter the nonlinear phase at very low amplitude (when the island width is comparable to the thin resistive layer), the results of our approach are relevant since it is known that nonlinear effects do not substantially change the threshold of instability, $\Delta' = 0$ [19, 20].

Considerable attention has been devoted to the study of stability properties of plasmas with flows. Rigid plasma rotation has been shown to have mitigating effects on resistive wall MHD instabilities [21, 22]. Previous work on tearing modes with sheared equilibrium flows [23–31] considered flows centred at the mode rational surface with shear inside the resistive layer, and focused on how the flow changes the scaling of the growth rate. Some of these works also point out the possible important influence of shear flow on Δ' [23, 31]. A detailed study of this latter issue was carried out in [32]. There, the reduced ideal MHD equations, valid for a tokamak field configuration ($B_z = \text{const.} \gg B_\theta$), were solved numerically in cylindrical geometry, and Δ' for tearing modes was calculated for large-scale plasma rotations. Although the approach followed in this work is similar to the approach of [32], it differs in at least two important respects. First, we consider a configuration in which both the equilibrium fields B_θ and B_z are radially dependent, as is the case for the RFP. This calls for a solution of the full ideal MHD system. Secondly, we

consider both localized and global regions of flow shear, while only the global case was considered in [32]. Our research goal is specific to the RFP, to wit, we seek to understand global resistive stability under the equilibrium magnetic field profiles and the geometric parameters representative of spontaneous EC discharges in MST. Because the situation with flow shear in a resistive layer has been studied, we focus on cases where flow within the resistive layer is nearly uniform, and shear is restricted to outer regions.

The principal result of this work is that both a narrow region of flow shear localized outside the reversal radius, and a global flow with nonzero shear in the middle region of the plasma (the latter defined to be the region between the $m = 1$, $n = -6$ rational surface and the reversal radius), increase Δ' of both core and edge tearing modes in the spontaneous EC regime. Of particular relevance is the fact that an edge-localized region of flow shear of sufficient strength destabilizes the $m = 0$ mode. This finding could offer an explanation for the periodic $m = 0$ activity observed during the spontaneous EC regime. The cycle associated with $m = 0$ bursts can be viewed as a relaxation oscillation regulated by the competition between the destabilization induced by the shear flow (possibly in combination with current density and pressure gradient effects), and the diffusion properties of the equilibrium. Moreover, we notice that if the ideal MHD results obtained in this paper are complemented with available results on inner-layer (resistive) effects, a possible explanation emerges as to why states in which the fluctuation spectrum is dominated by the innermost resonant $m = 1$ mode (QSH states) are sometimes observed in MST discharges.

In the following two sections we present the mathematical model which is used in the remainder of the paper. In particular, in section 2 we present the equation for the perturbed radial magnetic field in the outer region, and include an equilibrium flow. In section 3 we summarize the derivation of the stability factor, and discuss how the flow alters the static result. In section 4 we present the results of numerical calculations to determine the influence of an axial flow on the stability of both $m = 1$ and $m = 0$ modes in MST. We use magnetic equilibrium profiles which are derived from experimental data relative to a spontaneous EC discharge. Two classes of flow profiles are used. The first class encompasses flow profiles which are of narrow extent and localized in the outer region of the plasma, while the second class includes a broad flow profile with shear in the middle region of the plasma. In both cases, the flow inside the resistive layer of the mode under consideration is taken to have zero or negligible shear. The numerical results are discussed further in section 5 and compared to an analytical expression for the stability factor. The analytic results support the numerical results and clarify how the characteristics of a flow profile affect the stability of the mode. Finally, in section 6 we show that our results could offer possible explanations for some characteristic features of spontaneous EC regimes in MST.

2. Ideal MHD equation for the perturbing radial magnetic field

The linear stability of resistive modes can be calculated by solving the ideal MHD equations [33]. This is due to the fact

that resistivity, which creates a magnetic island, is important only in a thin layer around the rational surface (inner layer), while the free energy driving the instability comes mainly from the equilibrium quantities over the remaining plasma cross-section (outer region), where nonideal effects play a negligible role.

We approximate the MHD system assuming incompressibility and constant density,

$$\rho = \text{const.}, \quad \nabla \cdot \mathbf{V} = 0, \quad \nabla \cdot \mathbf{B} = 0, \quad (1)$$

$$\rho \left[\frac{\partial \mathbf{V}}{\partial t} + (\mathbf{V} \cdot \nabla) \mathbf{V} \right] + \nabla p - \mathbf{J} \times \mathbf{B} = 0, \quad (2)$$

$$\mu_0 \mathbf{J} = \nabla \times \mathbf{B}, \quad \frac{\partial \mathbf{B}}{\partial t} = -\nabla \times \mathbf{E}, \quad \mathbf{E} = -\mathbf{V} \times \mathbf{B}. \quad (3)$$

In cylindrical geometry (r, θ, z) , and for equilibrium fields of the form

$$\mathbf{B}(r, \theta, t) = B_\theta(r) \hat{\boldsymbol{\theta}} + B_z(r) \hat{\mathbf{z}},$$

$$\mathbf{V}(r, \theta, t) = V_\theta(r) \hat{\boldsymbol{\theta}} + V_z(r) \hat{\mathbf{z}},$$

the radial component of the momentum equation, which describes the linear plasma equilibrium, is given by

$$V_\theta^2 = \frac{r}{\rho} \frac{dp}{dr} + \frac{B_\theta^2}{\rho \mu_0} + \frac{r}{2\rho \mu_0} \frac{dB^2}{dr}, \quad (4)$$

where $B^2 = B_\theta^2 + B_z^2$. Note that only the poloidal component of the velocity is present in the radial force balance, due to the axial symmetry of the cylindrical system. As first described in [34] for static equilibria, the linearized versions of equations (1)–(3) can be combined into a single second-order equation for the radial magnetic perturbation \tilde{B}_r . We write this equation as

$$\frac{d^2 \tilde{B}_r(r)}{dr^2} + C(r) \frac{d\tilde{B}_r(r)}{dr} + D(r) \tilde{B}_r(r) = 0, \quad (5)$$

where we have assumed for any perturbed quantity $\hat{a}(r, \theta, z; t)$ the form $\tilde{a}(r) \exp[i(m\theta + k_z z + \omega t)]$. Besides radial dependence, the two coefficients in equation (5) depend on the poloidal mode number m , the axial wavevector k_z , and the frequency ω . To give concise expressions for these coefficients, we introduce the following radially dependent quantities:

$$F = \mathbf{k} \cdot \mathbf{B}, \quad G = \mathbf{k} \cdot \mathbf{V}, \quad V^2 = V_\theta^2 + V_z^2, \\ \Omega = \omega + G, \quad \Upsilon = \frac{(\mu_0 \rho)^{1/2} \Omega}{F}, \quad (6)$$

$$M_{l_\theta, l_z} = l_\theta m^2 + l_z k_z^2 r^2, \quad H = \frac{r^3(1 - \Upsilon^2)}{M_{1,1}},$$

and

$$\mathcal{F} = \frac{m}{r} B_\theta \left[\frac{M_{1,1}}{m^2(1 - \Upsilon^2)} - \frac{k_z^2 r^2}{m^2} \right] + k_z B_z,$$

where l_θ, l_z are positive integers. The coefficients of equation (5) can then be succinctly written as

$$C = \frac{1}{H} \frac{dH}{dr}, \quad D = g - \frac{1}{HF} \frac{d}{dr} \left(H \frac{dF}{dr} \right), \quad (7)$$

where

$$g = -\frac{m^2 - 1}{r^2} - \frac{k_z^2}{rF^2} \left\{ \left[\frac{2\mu_0}{(1 - \Upsilon^2)} \frac{dp}{dr} + rF^2 \right. \right. \\ \left. \left. + F \frac{2[rk_z B_z - mB_\theta \{2\mathcal{F}/[F(1 - \Upsilon^2)] - 1\}]}{M_{1,1}} \right] \right\} \\ - \frac{2\mu_0 \rho}{r^2 F^2 (1 - \Upsilon^2)} \left\{ r \left[\frac{d\Omega}{dr} \left(\Omega - \frac{m}{r} V_\theta \right) \right. \right. \\ \left. \left. + \frac{dV_\theta}{dr} \left(\frac{M_{1,1}}{r^2} V_\theta - \frac{m}{r} \Omega \right) \right] + \frac{m}{r} V_\theta \left(\Omega \frac{M_{1,3}}{M_{1,1}} - \frac{m}{r} V_\theta \right) \right. \\ \left. - \frac{2k_z^2 V_\theta (V_\theta F - 2B_\theta \Omega)}{F(1 - \Upsilon^2)} \right\}. \quad (8)$$

The dependence on the equilibrium flow of the coefficient C and the second term in D is made more explicit by rewriting them as

$$\frac{1}{H} \frac{dH}{dr} = \frac{M_{3,1}}{rM_{1,1}} - \frac{1}{(1 - \Upsilon^2)} \frac{d\Upsilon^2}{dr}$$

and

$$-\frac{1}{HF} \frac{d}{dr} \left(H \frac{dF}{dr} \right) = -\frac{1}{F} \left(\frac{M_{3,1}}{rM_{1,1}} \frac{dF}{dr} + \frac{d^2 F}{dr^2} \right) \\ + \frac{1}{F(1 - \Upsilon^2)} \frac{dF}{dr} \frac{d\Upsilon^2}{dr}.$$

It is easy to verify that the coefficients in equation (7) reduce to those of [35] when the equilibrium flow is zero. Indeed, noting that $\Upsilon \rightarrow 0$ when $\Omega = G = \omega = 0$ (where, as discussed later in the section, we set $\omega = -G(r_s)$), H reduces to the no-flow expression of [35]. The first two terms in g are seen to reduce to the expressions in [35] once it is noted that in the flowless case $(1 - \Upsilon^2) \rightarrow 1$, $\mathcal{F} \rightarrow F$ and $2\mathcal{F}/[F(1 - \Upsilon^2)] - 1 \rightarrow 1$. The remaining terms in g vanish.

The frequency ω present in equation (5) is in general a complex number, $\omega = \omega_R - i\gamma$, with ω_R and γ real quantities. In the remainder of the paper we will assume that the growth rate γ of the resistive perturbation scales as $\gamma \propto 1/S^\sigma$ with $0 < \sigma < 1$ (S being the usual ratio of the resistive diffusion and Alfvén times). In the ideal region $S \rightarrow \infty$, and thus the terms containing γ are of higher order and can be dropped, in the same way the resistive terms are excluded. Note that this makes Ω real (and hence the entire equation (5)). Moreover, with regard to the real part of the frequency ω_R , we will set $\omega_R = -\mathbf{k} \cdot \mathbf{V}|_{r=r_s}$, i.e. we shift to a reference frame in which the mode does not propagate at $r = r_s$. This is done for convenience, and does not influence the results of the stability calculations.

We end this section by briefly discussing the singularities present in the coefficients C and D . First we note that $C \propto 1/[rM_{1,1}(1 - \Upsilon^2)]$ and $D \propto 1/[r^5 M_{1,1} F^3 (1 - \Upsilon^2)^2]$, where $M_{1,1}$ (defined in equation (6)) is a positive definite function. Introducing $\mathbf{U} \equiv \mathbf{V}(r) - \mathbf{V}(r_s)$ and the Alfvén velocity $\mathbf{V}_A = \mathbf{B}/(\mu_0 \rho)^{1/2}$, the parameter Υ can be recast as $\Upsilon = \mathbf{k} \cdot \mathbf{U}/\mathbf{k} \cdot \mathbf{V}_A$. Noting that both $\mathbf{k} \cdot \mathbf{U}$ and $\mathbf{k} \cdot \mathbf{B}$ vanish at the rational surface, Υ is a measure of the shear in the flow profile relative to the shear in the magnetic field. If the two shear lengths are comparable, Υ^2 is proportional to the ratio of the kinetic to magnetic energy in the plasma. The location r_s

of the rational surface, where $F(r = r_s) = 0$, defines the usual resistive singularity, which is removed by any finite amount of resistivity. Additional singularities associated with the presence of the flow occur at the points $r = \tilde{r}_s$ where $\Upsilon^2 = 1$. This condition identifies the Alfvén continuum associated with a modified (i.e. with flow) Kelvin–Helmholtz ideal singularity. These singularities, which are quite different in nature from the one at the rational surface, have been discussed in [32]. In the present work we consider only flow profiles which do not lead to these additional singularities (i.e. $0 \leq \Upsilon^2 < 1$). Especially for flow profiles close to the rational surface of the mode, this will limit the magnitude of the velocity and thus of the strength of the shear present in the flow. In all cases, however, the magnitude of the velocities used in the calculations are not less than those experimentally observed in RFP plasmas.

3. Stability parameter Δ'

The criterion for the stability of classical tearing modes in the absence of flows and pressure gradient is given by [33, 35]

$$\Delta' \equiv \lim_{\epsilon \rightarrow 0} \left[\frac{1}{\tilde{B}_r(+\epsilon)} \left. \frac{d\tilde{B}_r}{dx} \right|_{x=+\epsilon} - \frac{1}{\tilde{B}_r(-\epsilon)} \left. \frac{d\tilde{B}_r}{dx} \right|_{x=-\epsilon} \right] < 0, \quad (9)$$

where \tilde{B}_r is the solution of equation (5) which satisfies the appropriate boundary conditions at $r = 0$ and at the plasma minor radius $r = a$. This solution is singular at the location $r = r_s$ where $F = 0$, and it is necessary to take a limit to eliminate this singularity and obtain a finite value for Δ' . Physically we can understand condition (9) by noting that Δ' , the discontinuity of \tilde{B}'_r across the inner region, is a measure of the magnetic energy to be gained by a perturbation producing a magnetic island at r_s . Hence a positive Δ' leads to instability. The procedure for finding \tilde{B}_r and the value of Δ' is summarized as follows [33]: (i) solve equation (5) numerically in the two regions $r = [0, r_s - \delta]$ and $r = [r_s + \delta, a]$ (where δ is a small positive number greater than the half-width of the resistive layer) as two separate initial value problems; (ii) find an analytical solution of equation (5) valid near $r = r_s$ (a solution that is fully specified by matching with the numerical solution at $r = r_s \pm \delta$); and (iii) using this analytical solution in equation (9), find the stability factor. As noted, in taking the limit the singular terms in the solution cancel out, leading to a finite value for Δ' .

To find the analytical solution, equation (5) is expanded around $x = r - r_s = 0$. To a good approximation we obtain (as discussed before, we are setting $\omega_R = -\mathbf{k} \cdot \mathbf{V}|_{r_s}$, i.e. $\Omega(r = r_s) = 0$)

$$\frac{d^2 \tilde{B}_r(x)}{dx^2} + \left(\frac{c_1}{x} + \frac{c_2}{x^2} \right) \tilde{B}_r(x) = 0, \quad (10)$$

where the coefficients c_1 and c_2 , which are evaluated at $r = r_s$, are rather complicated functions of equilibrium quantities. In the simple case of constant pressure and no flow, or flow only along the axial direction with $V'_z(r = r_s) = 0$, these coefficients reduce to

$$c_1 \rightarrow -\frac{M_{3,1}}{M_{1,1}r_s} - \frac{2k_z^2(r_s k_z B_z - m B_\theta)}{r_s M_{1,1} F'} - \frac{F''}{F'}, \quad c_2 \rightarrow 0. \quad (11)$$

The appropriate series solution, valid in the ideal region near the rational surface, is given in this case by

$$\tilde{B}_r^a(x) = \sum_{n=0}^{\infty} a_n x^n + \ln|x| \sum_{n=0}^{\infty} b_n x^n.$$

The coefficients of this series can be found by substituting the series into equation (10) and equating the terms with equal powers of x . We obtain

$$\begin{aligned} \tilde{B}_{r,L(R)}^a(x) &= \tilde{B}_s \left(1 - \frac{3}{4} c_1^2 x^2 + \frac{7}{36} c_1^3 x^3 - c_1 x \ln|x| \right. \\ &\quad \left. + \frac{c_1^2}{2} x^2 \ln|x| - \frac{c_1^3}{12} x^3 \ln|x| + \dots \right) \\ &\quad + \tilde{B}'_{s,L(R)} \left(x - \frac{c_1}{2} x^2 + \frac{c_1^2}{12} x^3 + \dots \right) + \mathcal{O}(x^2), \end{aligned} \quad (12)$$

where L and R mean to the left ($x < 0$) and right ($x > 0$) of the rational surface, respectively. Here we have set $b_0 = 0$ (\tilde{B}_r^a finite when $x \rightarrow 0$), $a_0 \equiv \tilde{B}_s$ (value of \tilde{B}_r^a at $x = 0$) and $a_1 \equiv \tilde{B}'_{s,L}$. Upon substituting equation (12) in equation (9), and taking the limit, the stability factor reduces to

$$\Delta' = \frac{\tilde{B}'_{s,R} - \tilde{B}'_{s,L}}{\tilde{B}_s}. \quad (13)$$

The matching at $x = -\delta$ between this analytical solution and the numerical solution of equation (5), $\tilde{B}_r^n(x = -\delta) = \tilde{B}_{r,L}^a(x = -\delta)$, $\tilde{B}_r^m(x = -\delta) = \tilde{B}_{r,L}^a(x = -\delta)$, allows the determination of the two constants \tilde{B}_s and $\tilde{B}'_{s,L}$, while the matching at $x = +\delta$, $C \tilde{B}_r^n(x = +\delta) = \tilde{B}_{r,R}^a(x = +\delta)$, $C \tilde{B}_r^m(x = +\delta) = \tilde{B}_{r,R}^a(x = +\delta)$, allows the determination of $\tilde{B}'_{s,R}$ and of the normalization constant C , the latter reflecting the linearity of the problem.

If $V_\theta \neq 0$ and/or $V'_z \neq 0$ at the rational surface, or if pressure effects are accounted for, the coefficient c_2 in equation (10) is nonzero. Because of the additional singular term $\propto 1/x^2$, the appropriate series solution is now of the form $\tilde{B}_r^a = |x|^\nu \sum_{n=0}^{\infty} A_n x^n$. When substituted into equation (10), two possible values for the index ν are found. The corresponding independent solutions are usually referred to as the small (subdominant) and large (dominant) solutions, due to their different behaviour [36]. Here we don't pursue further this case since in all the calculations that follow we consider only equilibria for which $c_1 \neq 0$, $c_2 = 0$. The appropriate expression for Δ' is then given by equation (13).

As observed, the criterion $\Delta' > 0$ ($\Delta' < 0$) for instability (stability) holds for classical, static tearing modes [35]. However, when flow parallel to the magnetic flux surfaces is present, unstable modes with $\Delta' < 0$ may exist [26]. Moreover other effects not considered in this work, like neoclassical effects [37], modify the stability criterion. Therefore, for the results presented in the remainder of this paper, the relevant quantity is the relative change in Δ' induced by the equilibrium flow. In the case of flows with no shear at the rational surface, as considered here, an increase (decrease) in Δ' always corresponds to a destabilization (stabilization) of the mode.

4. Numerical stability calculation with axial flow

We have numerically solved equation (5) to evaluate Δ' in the presence of various flow profiles characterized by a region of

shear. We have considered only flows in the axial direction. In the RFP configuration, flows localized at the outer edge of the plasma are mainly toroidal, while, even if not zero, poloidal flows in the central plasma region tend to be smaller in magnitude than toroidal flows. The equation has been nondimensionalized, using as reference quantities the minor radius and the values of the magnetic field and the Alfvén velocity on axis. It has been integrated as an initial value problem in the two regions $r = [0, r_s - \delta]$ and $r = [r_s + \delta, a]$, where δ is a small positive quantity better defined later in this section. The numerical solver, taken from the Numerical Algorithms Group (NAG) library available on the National Energy Research Scientific Computing Center (NERSC), is based on a variable-order, variable-step Adams method. We have assumed a perfectly conducting wall at $r = a$, so that $\tilde{B}_r(a) = 0$. At the centre of the cylinder we adopt the regularity conditions $\tilde{B}_r \propto (1 + k_z^2 r^2)^{1/2}$, $\tilde{B}'_r \propto k_z^2 r / (1 + k_z^2 r^2)^{1/2}$ for $m = 1$, and $\tilde{B}_r \propto k_z r$, $\tilde{B}'_r \propto k_z$ for $m = 0$. As explained in the previous section, this numerical solution is matched with the series solutions to evaluate the stability factor Δ' .

The matching point between the series and the numerical solutions, i.e. the quantity δ , has been chosen so that at $x \equiv r - r_s = \pm\delta$ both solutions are accurate. To find the δ which is optimal for each Δ' computation, we perform the following steps. First we look for the maximum δ such that at $x = \pm\delta$ the percentage difference between the coefficient c_1/x of the expanded equation (equation (11)) and the corresponding coefficient of the unexpanded equation (D in equation (7)) is less than or equal to a fixed tolerance value (say 0.15%). Secondly, we verify that the round-off errors during the computation of the coefficients of the unexpanded equation (equation (5)) are still negligible as the location $x = \pm\delta$ is approached during the numerical integration. As an additional verification, we also check that near the rational surface the term proportional to the first derivative of \tilde{B} is negligible when compared with the term proportional to \tilde{B} . This has to be the case, since the former term has been dropped in the expanded equation (equation (10)). Once the quantity δ has been fixed, we proceed with the calculation of Δ' . We keep the number of terms in the series solution (equation (12)) that are necessary to have a converged value for Δ' .

The equilibrium profiles of the magnetic field used in the numerical calculations presented in the remainder of this work were constructed from a polynomial fit to experimental data of an MST spontaneous EC discharge. In particular, the equilibrium is deduced from the experimental values of two edge quantities, the reversal parameter $B_z(a)/\langle B_z \rangle$ and the pinch parameter $B_\theta(a)/\langle B_z \rangle$, where $\langle \dots \rangle$ represents a volume average, and a is the minor radius [38]. Although this method of reconstructing the equilibrium magnetic profiles is inherently approximate, it leads to profiles which capture the main large-scale features of real equilibria. The minor and major radii are respectively $a = 52$ and $R = 150$ cm. In figure 1 we present equilibrium profiles of B_z , B_θ , q and F , the latter for an $m = 1$, $n = -6$ mode. The toroidal field and the safety factor on axis are respectively 0.23 T and 0.17, and the reversal radius is located at $r_r = 38.93$ cm. Moreover, we assume a constant particle density equal to $n_0 = 1 \times 10^{19} \text{ m}^{-3}$. Note the deep reversal of the magnetic field, a characteristic of most low-current spontaneous EC discharges. We will

refer to this equilibrium as the spontaneous EC reference configuration. It will be the starting point for studying the influence of shear flow on Δ' . When no equilibrium flow is present, we have found $\Delta'_{m=0,n=-1} = -1.06$, $\Delta'_{m=1,n=-8} = -0.19$, $\Delta'_{m=1,n=-7} = +0.87$ and $\Delta'_{m=1,n=-6} = +3.74$ (here and in the remainder of the paper we report the nondimensional value of the stability factor, as obtained by multiplying it by r_s). Thus the $m = 0$ and the $m = 1$, $n = -8$ modes are stable, while the $n = -7$ and $n = -6$ helicities of the $m = 1$ mode are unstable, the latter being the most unstable. For these equilibrium profiles the $m = 1$, $n = -5$ mode is not resonant. Note that the $n = -1$ helicity is the least stable $m = 0$ mode. For example, the $m = 1$, $n = -20$ mode has been found to have $\Delta' = -8.26$. In figures 2 and 3 we present the radial magnetic field eigenfunctions for the $m = 0$ and the $m = 1$, $n = -6$ modes. Via the optimization procedure discussed earlier in this section we have found, for example, that the optimal matching location (to satisfy a percentage tolerance value $\leq 0.15\%$) for the $m = 1$, $n = -6$ mode is obtained for

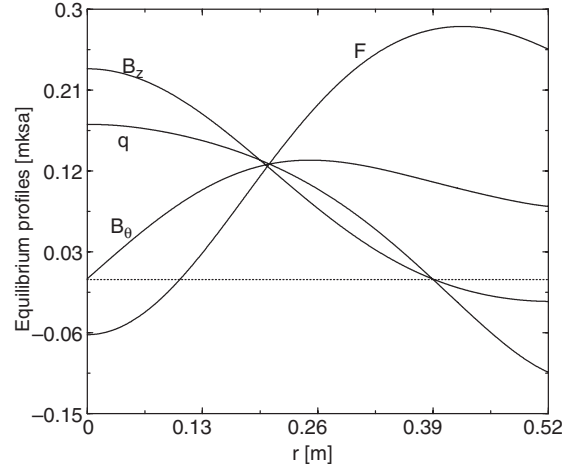


Figure 1. Axial magnetic field B_z (T), poloidal magnetic field B_θ (T), safety factor q (n.d.) and $F = \mathbf{k} \cdot \mathbf{B}$ (T/m) (the latter relative to the $m = 1$, $n = -6$ mode) equilibrium profiles (MST discharge no 275, 21 April 2000).

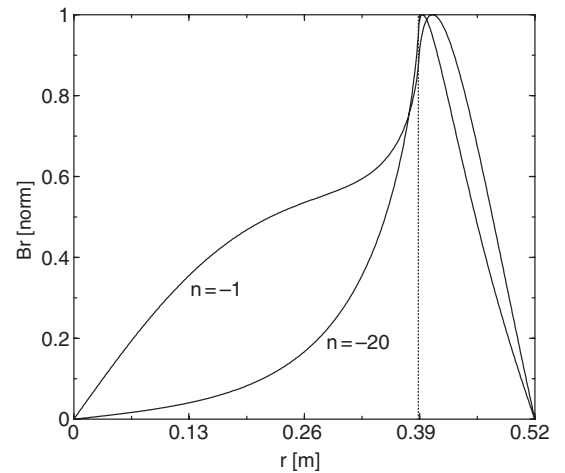


Figure 2. Perturbed radial magnetic field eigenfunction for $m = 0$ modes with no flow. The vertical line marks the location of the rational surface.

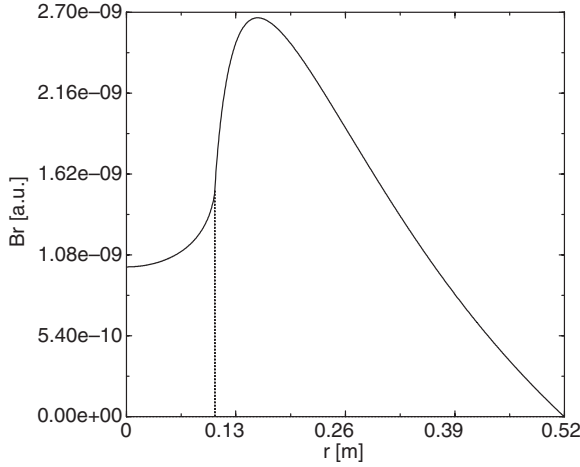


Figure 3. Perturbed radial magnetic field eigenfunction for the $m = 1, n = -6$ mode with no flow. The vertical line marks the location of the rational surface.

$\delta = 2.31 \times 10^{-4}$ m, and that only three terms in the series solution are needed to obtain a converged Δ' .

4.1. Stability of the $m = 1$ mode

The major contribution to magnetic fluctuations in MST comes from $m = 1$ core modes with toroidal mode number n ranging between -5 and -8 . For the spontaneous EC profiles presented in figure 1, the $n = -5$ mode is nonresonant. As we have found in the previous section, the most unstable mode is the $m = 1, n = -6$, resonant at $r_s = 10.51$ cm with $\Delta' = +3.74$. The flow profiles and intensities used in the numerical calculations have been selected with the present experimental knowledge of standard (low confinement) and spontaneous EC MST discharges in mind. This knowledge is briefly summarized as follows. The flow profile of a standard MST discharge appears to be monotonically decreasing from the plasma core to the edge. Core velocities are estimated to be around $10\text{--}20 \text{ Km s}^{-1}$, while at the edge the velocity drops to near zero or reverses direction, with a magnitude of few Km s^{-1} [39]. This global-scale flow profile is seen to persist during spontaneous EC discharges. In the latter, however, an additional edge-localized region of $E \times B$ flow, induced by a self-generated radial electric field, sets up outside the reversal radius. From the radial force balance equation, $E_r = \nabla p_i (n_i Z_i e)^{-1} - (\mathbf{V}_i \times \mathbf{B})_r$, and the available experimental data on the radial electric field, a rough estimate of the maximum toroidal rotation gives a lower bound of $V_\phi > E_r / B_\theta \simeq 65 \text{ Km s}^{-1}$ (assuming no pressure gradient and negligible poloidal rotation at the plasma edge) [40]. Guided by these data, we have performed Δ' calculations in the presence of an axial flow which is either confined in a narrow region on the outer edge of the plasma (see figure 4), or extends all across the plasma with shear confined in the middle region of the plasma (see figure 5). Note how both velocity profiles, the latter modelled by a hyperbolic tangent, have zero or negligible gradient at the location of both $m = 1, n = -6$ and $m = 0$ modes. Thus, neglecting pressure gradient effects, the appropriate formula for the stability factor is the one presented in equation (13). Notice that the edge-localized flows of

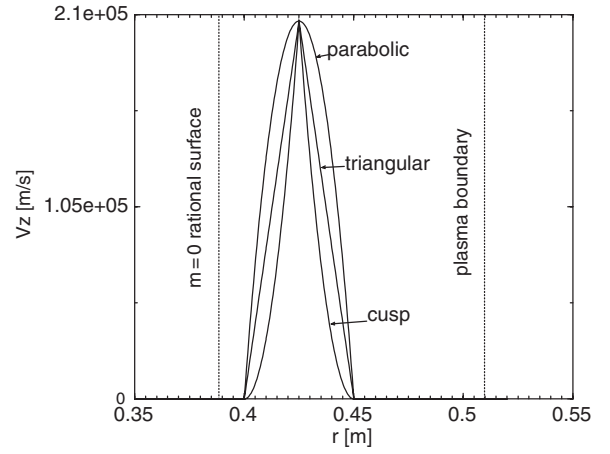


Figure 4. Edge-localized flow profiles used in the stability calculations (the centre location, width and magnitude of these flows have been varied in the numerical studies).

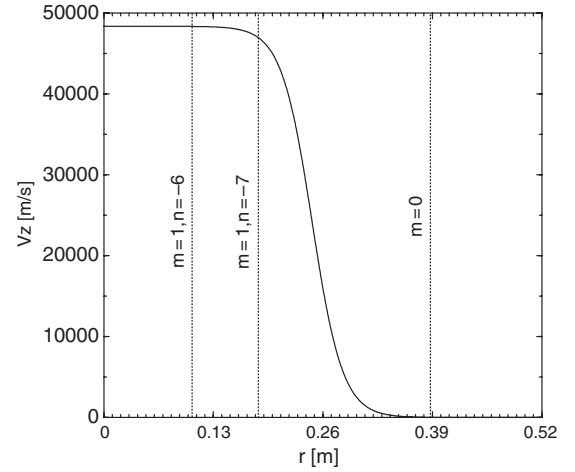


Figure 5. Global axial flow profile used in the stability calculations. The gradient of the flow is zero, or negligible, at the location of the rational surfaces.

figure 4 all have discontinuous first derivatives at the boundary of the flow region. As can be easily seen from equations (5) and (7), this feature does not preclude the smoothness of \tilde{B}_r (no second or higher derivatives of the flow are present in equation (5)). No particular precaution needs to be taken in numerically integrating across the boundaries of the region with flow, and the discontinuities in the flow do not invalidate the computed Δ' . The amplitudes of the velocities employed in the numerical calculations have been chosen to span a range of values that includes those relevant to experimental conditions. In some calculations, we have used values of the flow intensity that are above those experimentally observed. This has been done to establish trends; reducing these intensities to more realistic values does not change qualitatively the results.

Most of the present section will be devoted to the study of the influence of selected flow profiles on the stability of the $m = 1, n = -6$ mode for the spontaneous EC reference configuration. At the end of this section we will report results on the $m = 1$ modes with $n = -7, -8$ and $n = -9$. In the flowless case these helicities are stable, or much less unstable than the $n = -6$ helicity, and thus play a minor role in the

plasma dynamics. It is important to verify that this situation is not altered when plasma rotation is considered.

We explicitly note that a V_z flow which is constant everywhere in the plasma does not influence the stability of the mode. Similarly, a simple reversal of the direction of an axial flow ($V_z \rightarrow -V_z$) does not change the stability of the mode. These facts follow from the z -translational invariance of a cylindrical plasma. What is relevant is the sign (and magnitude) of the combination $V_z V_z'$.

In the first study we have considered the parabolic, triangular and cusp axial flow profiles shown in figure 4 as representative of localized flows. In the present case these flows are located outside the reversal radius between $r = 40$ and $r = 45$ cm. The magnitude of the flow at its central location ($r = 42.5$ cm) is $V_{z,\max} = 0.3 \times V_A \simeq 206 \text{ Km s}^{-1}$, where $V_A \simeq 688 \text{ Km s}^{-1}$ is the Alfvén velocity evaluated at the same location. We have found that these three flow profiles are all destabilizing, the stability factors being increased to, respectively, $\Delta' = +4.02$, $+3.90$ and $+3.83$ (corresponding to percentage increases of $(\Delta' - \Delta'_{\text{no flow}})/\Delta'_{\text{no flow}} \times 100 = 7.37$, 4.34 and 2.53%). If the maximum intensity of the flow is reduced to $\simeq 48 \text{ Km s}^{-1}$, the percentage increase in Δ' for the $n = -6$ helicity is reduced to 0.33% . In figure 6 we plot the corresponding \tilde{B}_r eigenfunctions across the outer region of the plasma. As seen from these plots, the eigenfunctions to the right of the rational surface are changed by the flow in such a way to increase their positive derivative at $r = r_s$. Since the eigenfunctions on the left side of the rational surface have remained unchanged, the stability factor Δ' increases. The reason why the parabolic profile is the most destabilizing of the three flows is mainly due to the fact that the velocity averaged over the region of flow is greater in the former case. Effects related to the different shape of the flow profiles are of secondary importance.

Next we have reconsidered the parabolic flow profile and performed two parametric studies to investigate how the intensity of the flow and its central location affect Δ' . The results are presented in figures 7 and 8. The first figure presents Δ' as a function of the parameter $(V_{z,\max}/L_V)/(V_A/a)$, where L_V is the width of the flow region, and $V_{z,\max}$ the intensity of the flow at its central location. This parameter is the natural extension of

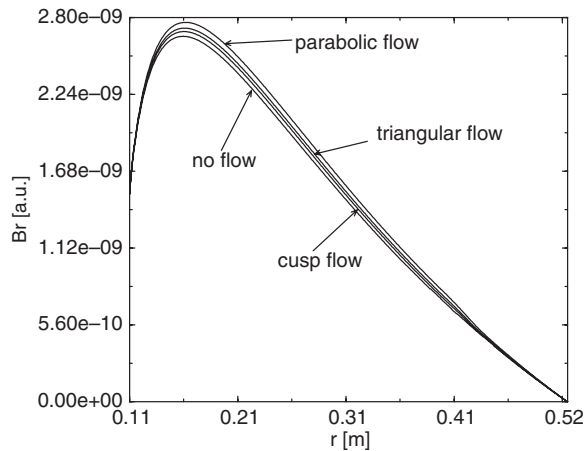


Figure 6. $m = 1$, $n = -6$ perturbed radial magnetic field eigenfunction for the parabolic, triangular, cusp and reference (no flow) cases.

the ratio $G'(r_s)/F'(r_s)$ to the case of a flow localized in the outer region. This ratio has been shown to be the relevant quantity in assessing the influence of an equilibrium flow inside the resistive layer on the stability of tearing modes (see, e.g. [31]). We see that the mode is increasingly destabilized as the intensity of the shear flow increases, the destabilization being roughly quadratic in $(V_{z,\max}/L_V)/(V_A/a)$. Figure 8 presents Δ' versus the centre location of the flow region. In this study the maximum intensity of the flow is held constant at $V_{\max} = 0.1 \times V_A \simeq 68 \text{ Km s}^{-1}$. We see that as the centre location is moved closer to the rational surface, the destabilizing action of the flow is more pronounced. As discussed in detail in the following section, this is due to the fact that the magnitude of the perturbed magnetic field eigenfunction overlapping with the region of flow shear increases as the latter approaches the resonant surface.

We perform a final numerical study to assess the influence of the broad flow profile of figure 5 on the stability of the $m = 1$, $n = -6$ mode. This broad flow profile is representative of the differential rotation that is observed in MST discharges. The rotation of the plasma increases in going from the edge to the centre of the plasma. We have evaluated the stability of the

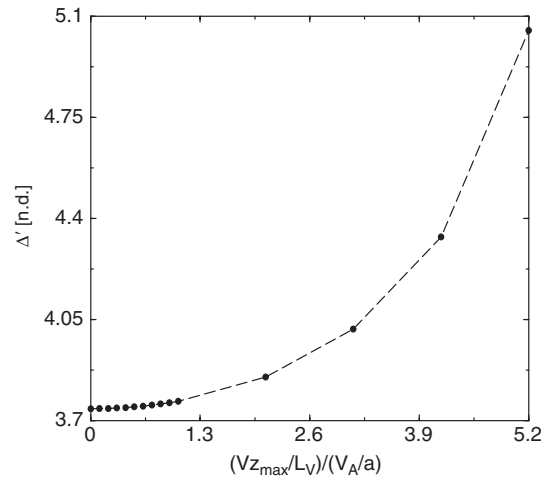


Figure 7. Stability factor of the $m = 1$, $n = -6$ mode vs the parameter $(V_{z,\max}/L_V)/(V_A/a)$ for an axial, edge-localized parabolic flow.

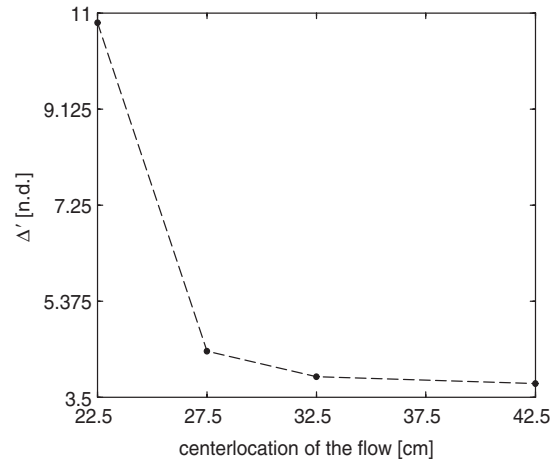


Figure 8. Stability factor of the $m = 1$, $n = -6$ mode vs the centre location of an axial, localized parabolic flow.

mode in the presence of such a flow, considering a maximum velocity (at $r = 0$) equal to $\simeq 48 \text{ Km s}^{-1}$. We have found that this flow is destabilizing, increasing the stability factor to $\Delta' = +4.50$, which corresponds to a 20.3% increase.

The other $m = 1$ helicity that is resonant and unstable is the $n = -7$. We have verified that a flow profile localized in the outer region of the plasma is destabilizing for the $m = 1$, $n = -7$ mode, as it is for the $n = -6$ mode. For example, the same parabolic axial flow that increases Δ' of the $n = -6$ mode by 7.37%, also increases Δ' of the $n = -7$ mode. In the latter case the increase is greater (15.8%), since the location of the rational surface of the $n = -7$ mode is closer to the region of flow shear. The effect of the global flow profile of figure 5 on the stability of the $n = -7$ mode is however potentially very different. The profile of figure 5 has two important features of relevance to this discussion: (1) the flow increases in going from the edge to the centre of the plasma, having the shear concentrated mainly in the middle region of the plasma, and (2) it has negligible shear at the locations of the $m = 1$, $n = -6$ and of the $m = 0$ modes. While the first feature is suggested by experimental data, the second feature of the profile allows us to compare the effect of the same global profile on the stability of both $m = 1$, $n = -6$ and $m = 0$ modes, for situations in which there is no stabilizing effect due to flow shear inside the resistive layer [31]. Avoiding resistive layer effects by the adoption of this tanh-like flow profile is realistic for the $n = -6$ mode, since near the centre of the plasma any axial flow profile is likely to have negligible shear for geometrical reasons. The situation is however different for the $n = -7$ mode. The rational surface of this mode is at $r_s = 18.12 \text{ cm}$, about 8 cm more toward the middle region of the plasma than the rational surface of the $n = -6$ mode. The $n = -7$ mode is then located right where a strong shear is expected, and effects related to the presence of shear flow inside the resistive layer need to be considered. In particular, it is known that if there is a strong shear flow inside the resistive layer of a mode, the mode is stabilized by inner layer effects, independent of the value of Δ' obtained with ideal MHD calculations [31]. Stabilization occurs whenever the quantity $\sqrt{\mu_0 \rho} G' / F'$ evaluated at the rational surface is greater than or equal to 1. From this consideration emerges the possibility that the global profile observed in spontaneous EC regimes could cause an increased destabilization of the $m = 1$, $n = -6$ mode (with respect to the flowless case), while stabilizing (or at least reducing the growth rate of) the $m = 1$, $n = -7$ mode. For example consider moving the location of the maximum shear of the hyperbolic tangent flow profile of figure 5 to the location of the $m = -1$, $n = -7$ mode rational surface, and increasing its central velocity up to $V_{z,\max} = V_z(r = 0) \simeq 203 \text{ Km s}^{-1}$ (0.13 of the value of the Alfvén velocity at the centre). The parameter $\sqrt{\mu_0 \rho} G' / F'$ evaluated for the $n = -6$ and the $n = -7$ modes corresponding to this modified tanh-like profile are, respectively, 0.0883 and 1.0002. Hence this profile increases the instability of the $n = -6$ mode (due to ideal effect), while it stabilizes, via inner layer effects, the $n = -7$ mode.

We conclude this section by considering the effect of the parabolic, edge-localized flow on the $m = 1$, $n = -8$ and $n = -9$ modes. In the absence of flow, these modes are linearly stable with $\Delta'_{n=-8} = -0.19$ and $\Delta'_{n=-9} = -0.98$. The 5 cm-wide parabolic flow profile centred at $r = 0.45 \text{ m}$

and of maximum intensity $V_{z,\max} = 0.3 \times V_A \simeq 206 \text{ Km s}^{-1}$ increases the stability factor of these two modes up to -0.02 and -0.72 , respectively. Despite its large intensity, this flow does not lead to destabilization of either mode.

In summary, we have found that both a broad flow profile with shear concentrated over the middle region of the plasma and a flow localized in the outer edge of the plasma further destabilizes the $m = 1$, $n = -6$ mode. A flow localized in the outer edge of the plasma further destabilizes the $m = 1$, $n = -7$, -8 , -9 modes, too. When considering the effect of a global flow profile on the $n \leq -7$ modes, however, results based on ideal MHD alone need to be integrated with a consideration of resistive effects. Since the location of the rational surface of these modes is located in a region of strong flow shear, resistive effects alone could stabilize these modes.

4.2. Stability of the $m = 0$ mode

In figure 2 we have presented the \tilde{B}_r eigenfunction for the $m = 0$, $n = -1$ mode under the reference equilibrium profiles presented in figure 1. The singular surface is located at the reversal radius, $r_s = r_r = 38.91 \text{ cm}$. As seen before, this mode is stable, with $\Delta'_{m=0} = -1.06$. This is the helicity (i.e. n number) of the $m = 0$ mode with the smallest (absolute) value of the stability factor.

We have repeated for the $m = 0$ mode the stability calculation for a flow localized in a narrow region between the mode resistive layer and the edge of the plasma. The flow profiles are centred at $r = 45 \text{ cm}$, and have a total width of $L_V = 4 \text{ cm}$. The centre location is thus located 6.06 cm to the right of the rational surface. As for the $m = 1$ case, we have considered the parabolic, triangular and cusp profiles. The maximum velocity has been set to $V_{z,\max} \simeq 52 \text{ Km s}^{-1}$. Like the $m = 1$ case, we have found that these localized flows are all destabilizing. However, since the $m = 0$ mode is stable in the absence of flow, the effect of the flow is more important than for the $m = 1$ case. In the latter case, the shear flow only increases the instability of a mode which is already unstable without flow. Moreover, the relative increase in Δ' is small since the flow is located far away from the rational surface. In the $m = 0$ case, the proximity of the flow to the rational surface leads to a strong destabilizing effect. The stability parameter goes from being negative to being positive, i.e. the flow drives a stable mode unstable. For example, the stability factor with the parabolic flow, which is the most destabilizing of these three flow profiles, is $\Delta' = +0.59$. To better quantify this important effect of a localized flow on the stability properties of the $m = 0$, $n = -1$ mode, we have reconsidered the parabolic flow profile and gradually increased its maximum intensity. The results of this parametric study are presented in figure 9. Interpolating these data, the marginal stability condition is obtained for a maximum flow of $\simeq 43 \text{ Km s}^{-1}$, or equivalently for $(V_{z,\max}/L_V)/(V_A/a) = 0.86$.

We have also repeated the broad flow profile study, as done for the $m = 1$ mode. The profile is the same one used for the $m = 1$ study (see figure 5). The velocity and its derivative are negligible at the location of the $m = 0$ rational surface. As with the corresponding $m = 1$ study, the maximum intensity of the flow has been set to $\simeq 48 \text{ Km s}^{-1}$. We have found that the value of the stability factor increases from -1.06 with no

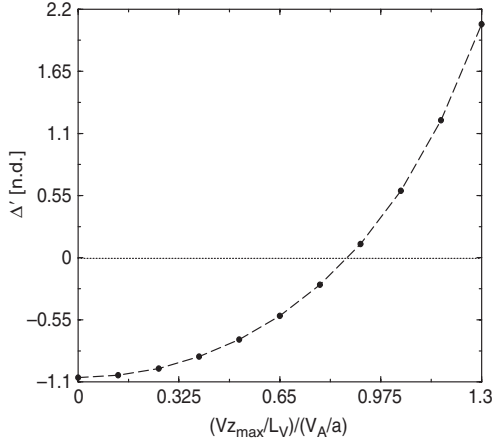


Figure 9. Stability factor of the $m = 0, n = -1$ vs the parameter $(V_{z,\max}/L_V)/(V_A/a)$ for an axial, edge-localized parabolic flow.

flow to -1.05 . In contrast to the $m = 1$ case, the stability of the $m = 0$ mode is almost unaffected by the flow. In the following section we will reconsider this result together with the corresponding result for the $m = 1$ mode, and show that their difference is explainable in terms of the relative location between the peak in the corresponding \tilde{B}_r eigenfunctions and the region of shear flow.

In summary, we have found that the $m = 0$ mode is strongly destabilized by a flow with shear which is localized to a narrow region at the outer edge of the plasma. This effect is important, since a flow with magnitude of the order of those experimentally observed in MST drives the $m = 0$ unstable. On the contrary, a tanh-like flow profile with shear in the region between the $m = 1, n = -6$ rational surface and the reversal radius does not change appreciably the stability factor of the $m = 0$ mode, and thus the mode remains stable even in the presence of the flow.

5. Analytical stability considerations

Due to the complicated way in which the equilibrium flow enters the coefficients (equation (7)) of equation (5), it is rather difficult to gather from them information on how a selected flow profile influences the stability of a mode. In this section we present an expression for Δ' which helps clarify how the characteristics of the flow influence the stability of tearing modes. To derive this result, we start from the generalization to cylindrical geometry of equation (60) in [23], which was derived in slab geometry. This equation is obtained by recasting equation (5) into a Schrödinger-like equation, a procedure which identifies the equivalent of the potential energy for the problem. In terms of the new dependent variable $\phi = r(1 - \Upsilon^2)^{1/2} \tilde{B}_r / M_{1,1}^{1/2}$, equation (5) is transformed into

$$\frac{1}{r} \frac{d}{dr} \left(r \frac{d\phi}{dr} \right) - U(r)\phi = K^2 \phi, \quad (14)$$

where $K^2 = m^2/r^2 + k_z^2$, and the potential U is given by

$$U(r) = -\frac{1}{r^2} + \frac{1}{F} \left(\frac{M_{3,1}}{rM_{1,1}} \frac{dF}{dr} + \frac{d^2F}{dr^2} \right) + \frac{m^2(m^2 - 2k_z^2 r^2)}{M_{1,1}^2 r^2} + \frac{k_z^2}{rF^2} \left\{ 2\mu_0 \frac{dp}{dr} + \frac{2F}{M_{1,1}} \left[rk_z B_z \right. \right.$$

$$\left. \left. - B_\theta \left(-2k_z r \frac{k_z B_\theta - (m/r) B_z}{F(1 - \Upsilon^2)} + \frac{2M_{1,1} B_\theta}{rF(1 - \Upsilon^2)^2} - m \right) \right] \right\} - \frac{2\mu_0 \rho k_z^2}{r^2 F^2 (1 - \Upsilon^2)} \left[\frac{2V_\theta}{(1 - \Upsilon^2)} \left(V_\theta - \frac{2\Omega B_\theta}{F} \right) - \frac{r}{2} \left(\frac{dV^2}{dr} + 4 \frac{m}{M_{1,1}} V_\theta \Omega \right) \right] - \frac{1}{2(1 - \Upsilon^2)} \left\{ \frac{d^2 \Upsilon^2}{dr^2} + \left[\frac{(d\Upsilon^2/dr)}{2(1 - \Upsilon^2)} + \frac{M_{3,1}}{rM_{1,1}} + \frac{1}{F^2} \frac{dF^2}{dr} \right] \frac{d\Upsilon^2}{dr} \right\}. \quad (15)$$

From this equation an expression for Δ' can be readily derived. Multiplying by ϕ , integrating by parts in the two regions $r = [0, r_s - \epsilon]$ and $r = [r_s + \epsilon, a]$ (with ϵ a small positive number), adding the resulting two equations, and finally taking the limit $\epsilon \rightarrow 0$, we obtain ($\int_0^a \equiv \lim_{\epsilon \rightarrow 0} (\int_0^{r_s - \epsilon} + \int_{r_s + \epsilon}^a)$)

$$-r_s \Delta' = \int_0^a dr r \left[\left(\frac{d\phi/dr}{\phi_s} \right)^2 + K^2 \left(\frac{\phi}{\phi_s} \right)^2 \right] + \int_0^a dr r U_0 \left(\frac{\phi}{\phi_s} \right)^2 + \int_0^a dr r U_1 \left(\frac{\phi}{\phi_s} \right)^2, \quad (16)$$

where $\phi_s = \phi(r_s)$, U_0 is the flowless part of the potential,

$$U_0 = -\frac{1}{r^2} + \frac{1}{F} \left(\frac{M_{3,1}}{rM_{1,1}} \frac{dF}{dr} + \frac{d^2F}{dr^2} \right) + \frac{m^2(m^2 - 2k_z^2 r^2)}{M_{1,1}^2 r^2} + \frac{k_z^2}{rF^2} \left\{ 2\mu_0 \frac{dp}{dr} + \frac{2F}{M_{1,1}} \left[rk_z B_z - B_\theta \left(-\frac{2k_z r [k_z B_\theta - (m/r) B_z]}{F} + \frac{2M_{1,1} B_\theta}{rF} - m \right) \right] \right\},$$

and $U_1 \equiv U - U_0$ is the remaining part of the potential that is nonzero only in the presence of flow. The latter can be conveniently divided into two contributions,

$$U_1(r) = U_{1,1} + U_{1,2}, \quad (17)$$

where

$$U_{1,1} = \frac{1}{(1 - \Upsilon^2)} \left\{ - \left[\left(\frac{1}{F} \frac{dF}{dr} + \frac{M_{3,1}}{2rM_{1,1}} \right) + \frac{1}{4(1 - \Upsilon^2)} \frac{d\Upsilon^2}{dr} \right] \frac{d\Upsilon^2}{dr} + \frac{\mu_0 \rho k_z^2}{rF^2} \frac{dV^2}{dr} - \frac{1}{2} \frac{d^2 \Upsilon^2}{dr^2} \right\}$$

contains only derivatives of the flow, and

$$U_{1,2} = \frac{2k_z^2}{rF^2(1 - \Upsilon^2)} \left\{ \left[\mu_0 \frac{dp}{dr} + \frac{2rk_z B_\theta (k_z B_\theta - (m/r) B_z)}{M_{1,1}} - \frac{2B_\theta^2 (2 - \Upsilon^2)}{r(1 - \Upsilon^2)} \right] \Upsilon^2 - 2\mu_0 \rho V_\theta \left[\frac{1}{r(1 - \Upsilon^2)} \times \left(V_\theta - \frac{2\Omega B_\theta}{F} \right) - \frac{m}{M_{1,1} \Omega} \right] \right\}.$$

In deriving equation (16), we have assumed that the function ϕ/\tilde{B}_r and its first derivative are continuous functions of r near r_s . This has been the case for all flow profiles used in the numerical simulations presented in this paper. Looking at equation (16), we notice that the first integral is always stabilizing, its integrand being a positive definite function. The remaining two integrals can be both stabilizing or destabilizing, depending on whether their integrands are positive or negative, respectively. The $(d^2F/dr^2)/F$ term in U_0 , which is the only

one surviving in slab geometry (except for the pressure gradient term), contains the destabilizing effect of the current density gradient. In figure 10 we plot the function $r \times U_0 \times (\phi/\phi_s)^2$, i.e. the integrand in the second integral in equation (16) for the $m = 1, n = -6$ mode in the reference configuration with no flow. The current density destabilization effect included in U_0 occurs to the right of the rational surface, where the second integral in equation (16) is negative. The major destabilization contribution occurs near the location of the singular surface, where the \tilde{B}_r eigenfunction peaks (see figure 3). From equation (16) it is apparent that, since $(\phi/\phi_s)^2$ is a positive function, the local criterion for flow stabilization is $U_1 > 0$. Note however that this is true only for small flows, i.e. for $\Upsilon^2 \ll 1$. When this condition is not satisfied, the modifications induced by the flow to the eigenfunction ϕ itself could change the values of the first two integrals in equation (16) in such a way to increase/decrease Δ' even for a U_1 which is positive/negative everywhere. Other than through the positive factor $(1 - \Upsilon^2)$ and the term directly proportional to dV^2/dr , the flow enters in $U_{1,1}$ through the first and second derivatives of Υ^2 . These derivatives can be expressed in terms of Ω and F as follows:

$$\frac{d\Upsilon^2}{dr} = 2\Upsilon^2 \left(\frac{1}{\Omega} \frac{d\Omega}{dr} - \frac{1}{F} \frac{dF}{dr} \right),$$

$$\frac{d^2\Upsilon^2}{dr^2} = 2\Upsilon^2 \left[\left(\frac{1}{F} \frac{dF}{dr} - \frac{1}{\Omega} \frac{d\Omega}{dr} \right) \left(3 \frac{1}{F} \frac{dF}{dr} - \frac{1}{\Omega} \frac{d\Omega}{dr} \right) - \left(\frac{1}{F} \frac{d^2F}{dr^2} - \frac{1}{\Omega} \frac{d^2\Omega}{dr^2} \right) \right],$$

where

$$\frac{d\Omega}{dr} = \frac{m}{r} \left(\frac{dV_\theta}{dr} - \frac{V_\theta}{r} \right) + k_z \frac{dV_z}{dr},$$

$$\frac{d^2\Omega}{dr^2} = \frac{m}{r} \left[\frac{d^2V_\theta}{dr^2} - \frac{2}{r} \left(\frac{dV_\theta}{dr} - \frac{V_\theta}{r} \right) \right] + k_z \frac{d^2V_z}{dr^2}.$$

Note how only V_z enters these expressions when $m = 0$.

As just observed, in the case in which $\Upsilon^2 \ll 1$, the plot of the function $r \times U_1$ in the region of shear flow gives precise indications on where the flow is stabilizing or destabilizing according to where $r \times U_1$ is positive or negative. Combined

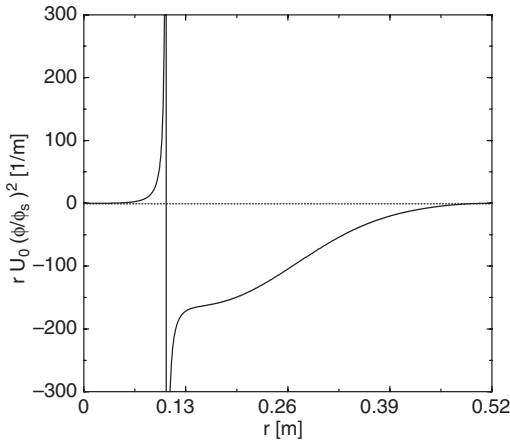


Figure 10. The function $r \times U_0 \times (\phi/\phi_s)^2$ for the $m = 1, n = -6$ mode of the reference configuration with no flow.

with the fact that the remaining term in the integrand is a positive definite function which tends to be monotonically decreasing sufficiently away from the rational surface of the mode, an indication could also be gained about the magnitude of stabilization or destabilization of a given flow profile. As an example, we reconsider the case of an axial flow profile localized in the outer region of the plasma between the reversal radius and the minor radius, and check if the information based on the potential energy just formulated supports the result obtained by the numerical computation of the stability factor for the $m = 0, n = -1$ mode. The information will be gleaned from plots of the potential energy associated with the flow. The localized flows considered before all have discontinuous derivatives at the boundary of the flow region. Although this feature does not preclude the smoothness of \tilde{B}_r , it would lead to nonrealistically discontinuous curves for the total potential energy. To avoid this, we select for the following study a Gaussian profile. This profile is centred at $r = 0.45$ m, has a half-width equal to 1.06 cm, and has a maximum velocity of $V_{z,\max} \simeq 52 \text{ Km s}^{-1}$. Similarly to the parabolic profile, we find that this Gaussian profile is destabilizing. The stability factor goes from -1.06 to $+0.35$, i.e. the mode is driven unstable. In figures 11 and 12 we plot respectively the functions $r \times U_1$ and $r \times U_1 \times (\phi/\phi_s)^2$, and $(\phi/\phi_s)^2$ associated with this flow. From

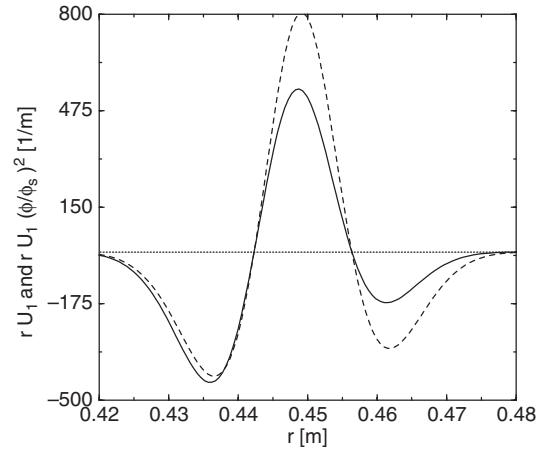


Figure 11. The functions $r \times U_1$ (---) and $r \times U_1 \times (\phi/\phi_s)^2$ (—) for the Gaussian flow profile.

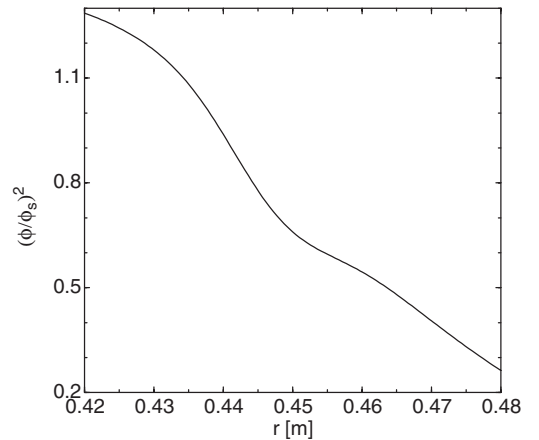


Figure 12. The function $(\phi/\phi_s)^2$ for the Gaussian flow profile.

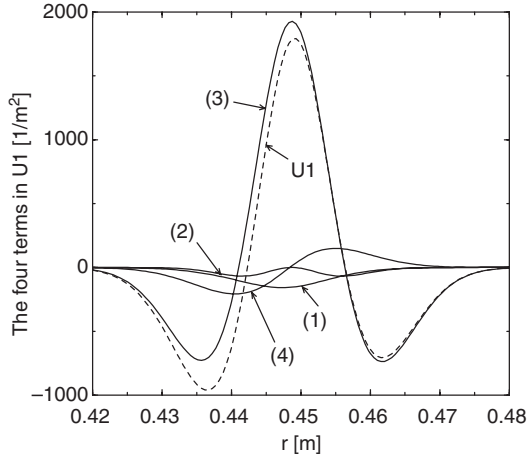


Figure 13. The four terms in U_1 for the Gaussian flow profile.

the first figure we see that the function $r \times U_1$ is negative near the edge of the flow region, giving destabilizing contributions, and becomes positive in the central region of the flow profile, giving a stabilizing contribution. The net effect is destabilizing. (The total area under the curve is -1.07 .) Moreover, the plot of the weighting function $(\phi/\phi_s)^2$ (figure 12) shows how in the integration the central stabilizing region of the flow is weighted much less than the left-edge destabilizing region. This is evident from the plot of the complete integrand (the solid line in figure 11): the extent of the central stabilizing region is reduced. Since the last integral in equation (16) is negative (the total area under the curve is -1.88), the parabolic flow profile is destabilizing, as found numerically. (The reason why Δ' increases by only $1.41 < 1.88$ is because, as noted before, the intensity of the flow makes the \tilde{B}_r eigenfunctions with and without flow differ by a significant amount. As a consequence, the remaining integrals in equation (16) (the first two in the equation) give also a contribution to Δ' , even though the coefficients K^2 and U_0 do not explicitly contain the flow.) To better understand which features of the flow profile lead to destabilization, we further decompose $U_{1,1}$ into the following three contributions,

$$U_{1,1}(1) = \frac{1}{(1 - \Upsilon^2)} \left[- \left(\frac{1}{F} \frac{dF}{dr} + \frac{M_{3,1}}{2rM_{1,1}} \right) \frac{d\Upsilon^2}{dr} + \frac{\mu_0 \rho k_z^2}{rF^2} \frac{dV^2}{dr} \right],$$

$$U_{1,1}(2) = \frac{1}{4(1 - \Upsilon^2)^2} \left(\frac{d\Upsilon^2}{dr} \right)^2,$$

$$U_{1,1}(3) = - \frac{1}{2(1 - \Upsilon^2)} \frac{d^2\Upsilon^2}{dr^2},$$

and plot them, together with the remaining term $U_{1,2}$, in figure 13 (in the figure, the three terms in $U_{1,1}$ are labelled (1), (2) and (3), while $U_{1,2}$ is labelled (4)). It is evident from these curves that the major contribution to U_1 comes from $U_{1,1}(3)$, i.e. the term proportional to the second derivative of Υ^2 .

We terminate this section by reconsidering the global profile studies of the $m = 1$ and $m = 0$ modes. We have found that the flow profile presented in figure 5 is destabilizing for the $m = 1$ mode, while it leaves practically unchanged the

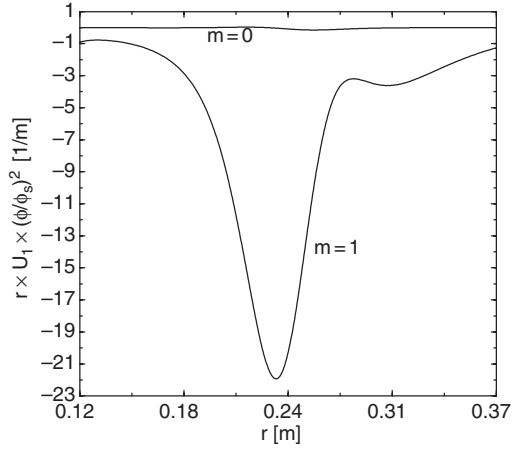


Figure 14. Comparison of the functions $r \times U_1 \times (\phi/\phi_s)^2$ for the $m = 0$ and $m = 1$ modes with global flow profile in the axial direction.

Δ' of the $m = 0$ mode. The reason for this difference can be seen from figure 14 where we plot the function $r \times U_1 \times (\phi/\phi_s)^2$ for the two cases. The areas under the two curves, although both negative, are quite different. The area under the $m = 0$ mode is much smaller than that of the $m = 1$ mode, as expected from the numerical results. This follows because the peak of the \tilde{B}_r eigenfunction occurs within the region of shear flow for the $m = 1$ case, while it occurs far away from it in the $m = 0$ case.

6. Summary and discussion

We have studied the linear stability of classical tearing modes for RFP equilibria with flows. To this end, a computer code that evaluates the linear stability parameter Δ' for the RFP has been developed. The code has been used to investigate the linear stability of both core- and edge-resonant tearing modes in spontaneous EC discharges in the MST. Among the characteristics of the spontaneous EC regime are a reduced level of magnetic fluctuations, the presence of an $E \times B$ shear flow localized at the edge of the plasma, and the occurrence of periodic bursts of $m = 0$ activity. Moreover, some spontaneous EC regimes enter a state in which the magnetic fluctuation spectrum is dominated by the innermost resonant $m = 1$ mode (QSH state). The magnetic field equilibrium used in the computations has been created by interpolating experimental profiles modelled for a discharge which had bifurcated into a spontaneous EC regime. To this equilibrium configuration we have added flows which are representative of those observed during spontaneous EC regimes. In particular, we have considered two classes of flow profiles. The first class consists of axial flows which are localized in a narrow region of the plasma outside the reversal radius. These flows are observed to form spontaneously right after a crash whenever the equilibrium bifurcates into a spontaneous EC regime. The second class of profiles consists of axial flows which are nonzero over most of the plasma, and have a shear localized mainly between the location of core and edge modes. This latter class of flows mimic the pattern observed between crashes in both standard and spontaneous EC discharges. Only immediately after the crash is this global flow pattern

temporarily modified: the rotation of the core mode slows down, and the plasma temporarily rotates quasirigidly. Note that a constant axial flow does not influence the stability of tearing modes.

For the spontaneous EC profiles used in the numerical calculation, and in the absence of equilibrium flows, the $m = 1$, $n = -5$ mode is not resonant, the $m = 1$, $n = -6$ and the $m = 1$, $n = -7$ modes are unstable (with $\Delta' = +3.74$ and $+0.87$ respectively), the $m = 1$, $n = -8$ and $n = -9$ are stable ($\Delta' = -0.19$ and -0.98 , respectively), and the $m = 0$, $n = -1$ mode is stable ($\Delta' = -1.06$). All the representative flow profiles considered in this paper (which have no or negligible shear in the inner layer of the mode) have been found to increase the stability factor Δ' of both core and edge tearing modes with respect to the static case. For example, an edge-localized parabolic flow profile 5 cm wide and of maximum velocity equal to $\simeq 48 \text{ Km s}^{-1}$ increases the stability factor of the $m = 1$, $n = -6$ mode by 0.33%, while a tanh-like global flow profile with the same maximum velocity increases it by 20.3%. This result indicates that the effect of an axial flow on the linear stability of the $m = 1$, $n = -6$ mode doesn't lead to substantial changes to the overall plasma characteristics, since it increases by a relatively small amount the stability factor of a mode which is already unstable without flow. Stability calculations for the $m = 1$, $n = -7$, -8 , -9 modes in the presence of an edge-localized flow show the analogous trend of Δ' increasing with flow shear. Despite this, we have found that the latter two helicities, which are stable without flow, do not become unstable under flows whose magnitudes are comparable to those of experiments. In contrast with the $n = -6$ case, however, a study of the effect of a global flow profile on the stability of the $n \leq -7$ modes (and in particular of the $n = -7$ mode, which is unstable in the static case) needs to include consideration of resistive effects, since the flow is likely to have a significant shear inside the inner layer of these modes. If this shear is sufficiently strong, resistive layer effects could lead to a stabilization of the $n = -7$ mode, independent of the value of Δ' . With regard to the $m = 0$, $n = -1$ mode we have found that, like the $m = 1$ case, both an edge-localized and a global axial flow add a positive contribution to the stability factor. However, this effect is notably more important than for core modes, since the $m = 0$ mode is stable in the absence of flow. In particular, while a global flow profile makes the mode less stable by a very small amount, a localized flow can reverse the sign of the stability factor, thus driving the mode linearly unstable. For example, a parabolic flow profile of maximum intensity of $\simeq 52 \text{ Km s}^{-1}$, 4 cm wide and with its centre located 6 cm to the right of the reversal radius increases the stability factor of the mode from the flowless value of -1.06 to $+0.59$.

We now discuss the possible implication of these findings, beginning with the result that the $m = 0$ mode can be driven unstable by a region of shear flow localized near the edge of the plasma. (The physics underlying the generation and maintenance of the edge-localized shear flow is not addressed here. Although various explanations have been proposed (in the RFP context, see for example [41, 42]), the problem remains, at present, open.) We speculate that the destabilization of the $m = 0$ mode by an edge-localized $E \times B$ axial shear flow could be related to the $m = 0$ bursts observed

in spontaneous EC discharges. To see how, we go back to equation (16). The most important terms in the flowless part of the potential, U_0 , are the drives associated with the current density and pressure gradients,

$$U_0 \propto +\frac{1}{F} \frac{d^2 F}{dr^2} + \frac{2\mu_0 k_z^2}{r F^2} \frac{dp}{dr}.$$

(The other terms in U_0 are related to geometrical effects, and are not present in slab geometry.) For the magnetic equilibrium profiles of figure 1 and a pressure profile monotonically decreasing with radius, these two terms are both destabilizing (negative). The other term in equation (16) which can be positive or negative is the U_1 term associated with the flow. As seen earlier, for an edge-localized flow this term is destabilizing (negative). On the basis of these considerations, it is seen that a time-dependent destabilization of the $m = 0$ mode could occur in two ways (or a combination of the two): U_1 oscillates in time while U_0 is constant, or U_0 oscillates in time while U_1 is constant. The first scenario could occur if the mechanism which generates the flow is periodic in nature, i.e. it is due to an instability which periodically reaches the instability threshold, and then decays due to some sort of quasilinear stabilization (as in a predator-prey instability model). If this is the case, the intensity of the flow generated by this instability could be oscillating in time, subject to periodic generation and viscous decay, ultimately leading to a periodic destabilization of the $m = 0$ mode. In particular, from our simulations we found that the maximum intensity of a parabolic flow centred at $r = 45 \text{ cm}$ and 4 cm wide which destabilizes the $m = 0$ mode is of the order of 40 Km s^{-1} . This value is only indicative, since small changes in the flow profile could change significantly this threshold value. We note that at present there are no experimental data which either prove or disprove a time dependence of the $E \times B$ shear flow of spontaneous EC discharges. Related data however indicate that a periodic time dependence of the flow is likely [40]. In the other scenario, the drive from the U_1 term is constant, i.e. it is due to an edge-localized flow which is stationary during the spontaneous EC regime. The required time dependence would then come from U_0 as follows. The initial creation of the flow region, which marks the transition to the spontaneous EC regime, destabilizes the $m = 0$ mode, according to the findings reported in figure 9. This leads to a rapid increase of magnetic turbulence around the location of the $m = 0$ rational surface, with consequent local flattening of the equilibrium profiles (both current density and pressure). This flattening is a fast process, tied to anomalous transport processes. Due to this profile modification, the drive introduced by U_0 diminishes, until the stability factor Δ' becomes negative, and the $m = 0$ mode is stabilized. This burst phase is followed by a slower ramp phase, during which classical diffusion processes ultimately restore the original equilibrium profiles. The cycle could then repeat itself. Note that this dynamics is like that of the sawtooth crash associated with the $m = 1$ mode [43]. The only difference is that in the case of the $m = 0$ bursts, the free energy driving the mode unstable is coming, according to our scenario, from a combination of the current density and pressure gradients, and the flow shear, whereas the current density gradient and the pressure gradient are the only factors for the $m = 1$ sawtooth cycle. Periodic bursts of $m = 0$ activity

are also observed during pulsed poloidal current drive (PPCD) MST plasmas [44]. PPCD plasmas are obtained by inducing auxiliary parallel current drive in the plasma edge, and present a significantly reduced level of $m = 1$ fluctuations. Also, recently a new induction technique that avoid the reversal of the surface parallel electric field has resulted in PPCD plasmas with no $m = 0$ bursts [45]. The cause of the $m = 0$ bursts nor the mechanism by which they are suppressed in PPCD plasmas is not yet established. However, we observe that manipulation of the edge electric field is very likely to strongly modify the local profile of the plasma rotation. The connection between the $m = 0$ activity and edge shear flow just discussed in the context of spontaneous EC discharges could apply to PPCD plasmas as well. With regard to the $m = 0$ bursts, we finally observe that, according to our calculation, all the $m = 1$ helicities which are stable in absence of flow ($n \leq -8$), are not destabilized by the edge-localized parabolic flow that destabilizes the $m = 0$ mode. We have found this to be true up to values of the maximum flow velocity that exceed the likely magnitude of experimental flows.

The equilibrium profiles used in the numerical calculations are characterized by a strong reversal of the toroidal magnetic field. Because of this, the edge-localized flows used in the simulations do not overlap with the resistive layer of the $m = 0$ mode. This seems to be the case for spontaneous EC regimes with total plasma current of about 200–250 kA. However, spontaneous EC regimes with higher plasma current tend to have a shallower reversal [15]. In these regimes, the $E \times B$ shear flow could be partially overlapping with the $m = 0$ inner layer, and stabilization due to resistivity effects could play a role.

Discharges with an externally induced $E \times B$ edge-localized flow shear have also been experimentally investigated in MST. These discharges show a reduction of edge-localized electrostatic fluctuations, but no $m = 0$ bursts or reduction in global magnetic fluctuations [46]. However, the maximum intensity of the shear flow induced so far in these regimes has been smaller than the shear flow of the spontaneous EC regimes. The speculations on a possible destabilization of the $m = 0$ mode by an edge shear flow are therefore not applicable to present biasing experiments.

A final observation regards QSH states. These states may be beneficial for RFP confinement in that they have a reduced level of magnetic stochasticity [47]. In the MST RFP, QSH states have been observed in both standard and improved-confinement discharges, and are usually characterized by a spectrum dominated by the innermost resonant $m = 1$ mode [48]. Except for the edge-localized $E \times B$ flow, standard, PPCD and spontaneous EC discharges in MST appear to have a similar large-scale rotation pattern. In section 4.1 we found that if inner layer effects are neglected, the tanh-like global flow profile of figure 5 further destabilizes the $n = -6$ helicity of the $m = 1$ mode. However, we have also noted there that, while a realistic flow profile would tend to have negligible shear near the centre of the plasma, where the $n = -6$ mode is located, it would have a significant amount of shear at the location of higher $m = 1$ helicities. In some discharges, the shear flow present inside the resistive layers of the $n \leq -7$ modes could be large enough to stabilize these modes (or at least to reduce their amplitudes), independent of the value of the stability parameter

based on ideal MHD calculations. A consideration of ideal and resistive effects of a global flow profile with significant shear in the middle region of the plasma (where the $m = 1$, $n \leq -7$ rational surfaces are located) thus suggests that a plasma state in which only the $m = 1$, $n = -6$ mode, i.e. the innermost resonant mode, is unstable (or at least dominates) is possible. QSH states in MST could then be explained by a consideration of shear flow effects on the stability of the tearing modes.

To conclude, we point out some facts regarding the validity and the limitations of the results presented in this work. The first point regards the intensity of the equilibrium flows. Sufficiently large flows can affect the equilibrium profiles, which in turn change the stability of the plasma. In our simplified geometry, this is however true only for poloidal flows. Axial flows, which have been considered in this work, do not enter the radial force balance equation and hence leave the equilibrium unchanged. Our results are thus not limited by this factor. More realistic geometries and/or inclusion of poloidal flows would require a self-consistent modification of the equilibrium. The stability of the plasma could also be affected directly by flow with intensities large enough to introduce the additional Alfvén-like singularities. This effect has been studied in [32]. We stress however that the flow intensities considered in our numerical calculation are consistent with experimental data; larger flows are unlikely to be realistic. Secondly, we observe again that, although our analysis is strictly linear and tearing modes enter the nonlinear phase at very low amplitude, there is evidence that nonlinear effects do not substantially change the threshold of instability, $\Delta' = 0$ [19, 20]. The results obtained in this work could then retain their value well into more realistic nonlinear regimes. A third source of approximation that is present in this work is the uncertainty in the adopted equilibrium magnetic profiles. As discussed in section 4, the method of constructing these profiles is based mainly on experimental data obtained at the edge of the plasma. Although the resulting profiles reproduce fairly well large-scale features of real discharge equilibria, they are not able to capture finer-scale features that might be relevant to the stability calculations presented in this work. Finally we stress that, at present, data on the intensity, location and profile of the flows present in MST discharges are still approximate. As a consequence, the model flow profiles used in our calculations have been chosen not only to reflect the (limited) experimental information presently available, but also for computational convenience. Until more definitive data are available, studies like the one presented here need to be considered as qualitative explorations of possible important scenarios, more than quantitative studies of realistic situations.

Acknowledgments

The authors would like to offer particular thanks to Brett Chapman and John Sarff for their reading of an earlier version of the manuscript and for their very useful comments and suggestions. The authors also acknowledge useful conversations with Darren Craig and Uday Shah on various topics related to this work, as well as help from Jay Anderson and Carl Sovinec on numerical aspects of this work. Finally, thanks are due to Scott Kruger for providing references on previous works on the subject. This work was supported by the US Department of Energy.

References

- [1] Stoneking M.R. *et al* 1994 *Phys. Rev. Lett.* **73** 549
- [2] Fiksel G., Prager S.C., Shen W. and Stoneking M.R. 1994 *Phys. Rev. Lett.* **72** 1028
- [3] Ji H. *et al* 1996 *Phys. Plasmas* **3** 1935
- [4] Watt R.G. and Nebel R.A. 1983 *Phys. Fluids* **26** 1168
- [5] Hokin S.A. 1991 *Phys. Fluids B* **3** 2241
- [6] Den Hartog D.J. *et al* 1995 *Phys. Plasmas* **2** 2281
- [7] Prager S.C. *et al* 1995 *Plasma Phys. Control. Fusion* **37** A303
- [8] Hegna C.C. 1996 *Phys. Plasmas* **3** 4646
- [9] Hansen A.K. *et al* 2000 *Phys. Rev. Lett.* **85** 3408
- [10] Terry P.W. and Fiksel G. 1998 *Transport Task Force Workshop (Atlanta, GA 1998)*
- [11] Turner M.F. and Wesson J.A. 1982 *Nucl. Fusion* **22** 1069
- [12] Diamond P.H., Hazeltine R.D., An Z.G., Carreras B.A. and Hicks H.R. 1984 *Phys. Fluids* **27** 1449
- [13] Taylor J.B. 1974 *Phys. Rev. Lett.* **33** 1139
- [14] Taylor J.B. 1986 *Rev. Mod. Phys.* **58** 741
- [15] Chapman B.E., Chiang C.-S., Prager S.C., Sarff J.S. and Stoneking M.R. 1998 *Phys. Rev. Lett.* **80** 2137
- [16] Chapman B.E. *et al* 1998 *Phys. Plasmas* **5** 1848
- [17] Dexter R.N., Kerst D.W., Lowell T.W., Prager S.C. and Sprott J.C. 1991 *Fusion Technol.* **19** 131
- [18] Groebner R.J., Burrell K.H. and Seraydarian R.P. 1990 *Phys. Rev. Lett.* **65** 3015
- [19] Rutherford P.H. 1973 *Phys. Fluids* **16** 1903
- [20] White R.B., Monticello D.A., Rosenbluth M.N. and Waddell B.V. 1977 *Phys. Fluids* **20** 8000
- [21] Gimblett C.G. 1986 *Nucl. Fusion* **26** 617
- [22] S  therblom H.-E., Schnack D.D. and Drake J.R. 1998 *Plasma Phys. Control. Fusion* **40** 1775
- [23] Hofmann I. 1975 *Plasma Phys.* **17** 143
- [24] Paris R.B. and Sy W.N.-C. 1983 *Phys. Fluids* **26** 2966
- [25] Dobrowolny M., Veltri P. and Mangeney A. 1983 *J. Plasma Phys.* **29** 303
- [26] Bondeson A. and Persson M. 1986 *Phys. Fluids* **29** 2997
- [27] Einaudi G. and Rubini F. 1986 *Phys. Fluids* **29** 2563
- [28] Persson M. and Bondeson A. 1990 *Phys. Fluids B* **2** 2315
- [29] Persson M. 1991 *Nucl. Fusion* **31** 382
- [30] Wang S., Lee L.C. and Wei C.Q. 1988 *Phys. Fluids* **31** 1544
- [31] Chen X.L. and Morrison P.J. 1990 *Phys. Fluids B* **2** 495
- [32] Wessen K.P. and Persson M. 1991 *J. Plasma Phys.* **45** 267
- [33] Furth H.P., Killeen J. and Rosenbluth M. 1963 *Phys. Fluids* **6** 459
- [34] Hain Von K. and L  st R. 1958 *Z. Naturforschg.* a **13** 936
- [35] Furth H.P., Rutherford P.H. and Selberg H. 1973 *Phys. Fluids* **16** 1054
- [36] Johnson J.L., Greene J.M. and Coppi B. 1963 *Phys. Fluids* **6** 1169
- [37] Hegna C.C. 1998 *Phys. Plasmas* **5** 1767
- [38] Antoni V., Martin P. and Ortolani S. 1989 *Nucl. Fusion* **29** 1759
- [39] Almagri A.F. *et al* 1998 *Phys. Plasmas* **5** 3982
- [40] Chapman B.E. 1997 Fluctuation reduction and enhanced confinement in the MST reversed-field pinch *PhD Dissertation* University of Wisconsin-Madison
- [41] Antoni V. *et al* 1997 *Phys. Rev. Lett.* **79** 4814
- [42] Bartiromo R. 1998 *Phys. Plasmas* **5** 3342
- [43] Terry P.W. *et al* 1997 *Plasma Physics and Controlled Nuclear Fusion Research* (1996) vol 2 (Vienna: International Atomic Energy Agency) p 665
- [44] Sarff J.S., Lanier N.E., Prager S.C. and Stoneking M.R. 1997 *Phys. Rev. Lett.* **78** 62
- [45] Chapman B.E. *et al* 2001 *Phys. Rev. Lett.* **87** 205001
- [46] Craig D. *et al* 1997 *Phys. Rev. Lett.* **79** 1865
- [47] Martin P. *et al* 2000 *Phys. Plasmas* **7** 1984
- [48] Martin P. *et al* 2001 *Controlled Fusion and Plasma Physics 2001, Proc. 28th Eur. Conf. Madeira, 2001* (Geneva: European Physical Society) P1.031
- Marrelli L. *et al* 2002 *Phys. Plasmas* in press